

Chiral and deconfinement transition from Dyson-Schwinger equations

Christian S. Fischer^{1,2} and Jens A. Mueller¹

¹*Institut für Kernphysik, Technische Universität Darmstadt, Schlossgartenstraße 9,
D-64289 Darmstadt, Germany*

²*GSI Helmholtzzentrum für Schwerionenforschung GmbH, Planckstr. 1 D-64291 Darmstadt, Germany.*

(Dated: October 28, 2018)

We determine the quark condensate and the dressed Polyakov loop from the finite temperature Landau gauge quark propagator evaluated with $U(1)$ -valued boundary conditions in an approximation to quenched QCD. These gauge invariant quantities allow for an investigation of the chiral and deconfinement transition. We compare results from Dyson-Schwinger equations on a lattice with infinite volume continuum results and study the temperature and quark mass dependence of both quantities. In particular we investigate the chiral condensate and the dressed Polyakov loop in the chiral limit. We also consider an alternative order parameter for the deconfinement transition, the dual scalar quark dressing, and compare with the dressed Polyakov loop. As a result we find only slightly different transition temperatures for the chiral and the deconfinement transition at finite quark masses; in the chiral limit both transitions coincide.

PACS numbers: 12.38.Aw, 12.38.Lg, 11.10.Wx

I. INTRODUCTION

The chiral and the deconfinement transition of QCD are a subject of continuous interest both, from a theoretical and from an experimental point of view. Ongoing experiments at the Relativistic Heavy Ion Collider (RHIC) and future runs at LHC and FAIR probe the transition between the high and low temperature states of strongly interacting quark matter. The transition is characterized by the breaking and restoration of chiral and center symmetry. Hereby it is well known that both transitions are phase transitions in the strict sense of the word only in opposite limits of the theory. In the chiral limit $m = 0$ chiral quantities such as the chiral condensate $\langle\bar{\psi}\psi\rangle$ or the scalar part $B(0)$ of the inverse quark propagator at zero momentum are order parameters of the chiral phase transition. In the absence of dynamical quarks, $m \rightarrow \infty$, pure gluonic systems are center symmetric in the low temperature phase. The deconfinement phase transition is then related to center symmetry breaking indicated by a non vanishing order parameter as e.g. the Polyakov loop L [1]. In the real world, quarks carry (light) masses and both transitions are crossovers as nicely established by lattice QCD, see e.g. [2, 3, 4, 5] and references therein.

The theoretical search for an underlying mechanism that links quark confinement and chiral symmetry breaking has brought many interesting results in the past years. Topological field configurations such as center vortices have been argued to connect both phenomena, see e.g. [6] for a review. In [7] a close connection between center vortices and the spectrum of the Dirac operator has been revealed; removing those vortices from the gauge field ensemble resulted in a vanishing string tension and a zero chiral condensate via the Casher-Banks relation.

Very recently a number of works [8, 9, 10, 11, 12, 13, 14, 15] have explored the relation between chiral and deconfinement signatures in the spectrum of the Dirac-

operator. In [11] it has been shown that the low lying eigenmodes of the Dirac operator are responsible for both, chiral symmetry breaking and confinement: spectral sums of the Dirac operator may be truncated to the lowest lying modes and still lead to a linear rising quark-antiquark potential extracted from the Polyakov-loop correlator.

One of these spectral sums, the dual condensate or dressed Polyakov loop, is of particular interest since it relates the chiral condensate to the Polyakov loop. This quantity has been studied in lattice gauge theory [12] and with Dyson-Schwinger equations on a torus [16] with qualitatively similar results. Both of these studies dealt with the dressed Polyakov loop on a compact manifold at finite quark masses. In this work we add more details to these investigations, in particular considering the infinite volume limit, the chiral limit and the large temperature behavior of these quantities. We also investigate another order parameter for the deconfinement transition, the dual scalar quark dressing function. Compared to Ref. [16] we also modified the renormalization condition of the quark mass function in the torus formulation, thus eliminating temperature effects in the bare quark mass. As a result we now obtain almost similar transition temperatures for the chiral and the deconfinement transition for quark masses roughly corresponding to an up-quark and identical transition temperatures in the chiral limit.

This work is organized as follows: In section II we outline our two order parameters for the confinement-deconfinement transition. Here we consider (i) the dual quark condensate as defined in Ref. [12] and (ii) the dual scalar quark dressing function as defined below. Both quantities share the property that they can be extracted from the momentum dependence of the quark propagator and are therefore accessible with functional methods. In this work we use the Dyson-Schwinger equations (DSEs) for the quark propagator in Landau gauge to determine these order parameters. The temperature dependence

of the propagator is evaluated in the Matsubara formalism. We employ a truncation scheme for the quark-DSE that uses $SU(2)$ -lattice results for the temperature dependent gluon propagator [17] and a temperature dependent ansatz for the quark-gluon vertex as input. This scheme is detailed in section III, where we also discuss our numerical procedure. In section IV we present our numerical results in the infinite volume/continuum formulation of the DSEs and compare with the results of Ref. [16] obtained from a formulation of the DSEs on a torus. Our infinite volume approach also enables us to explore the chiral limit of the theory. We compare results for the order parameters specified in section II and comment on relations to the chiral phase transition. Our results are summarized in the concluding section V. Throughout the paper we work in $SU(2)$ -Yang-Mills theory, leaving the $SU(3)$ case for future work.

II. ORDER PARAMETERS FOR DECONFINEMENT

Quantities that transform non trivial under center symmetry and thus qualify as order parameters for deconfinement are in general not easily accessible by functional methods. However, there has been considerable progress on this issue in the past years. In Ref. [18], the ghost and gluon propagators of Landau gauge Yang-Mills theory have been used to determine the Polyakov loop potential within an effective action approach. In this work we will focus on an alternative strategy that allows to extract chiral and deconfinement order parameters from a (generalized) quark propagator. This approach establishes links between dynamical chiral symmetry breaking and quark confinement in QCD. [8, 9, 10, 12, 16, 19].

A. The dual condensate

The dual quark condensate as order parameter for center symmetry has emerged from a series of works connecting spectral sums of the Dirac propagator with Polyakov loops and their correlators [8, 9, 10]. Within the framework of lattice gauge theory the dual condensate Σ_n has been introduced in Ref. [12]. It is defined by the phase-Fourier-transform

$$\Sigma_n = \int_0^{2\pi} \frac{d\varphi}{2\pi} e^{-i\varphi n} \langle \bar{\psi}\psi \rangle_\varphi \quad (1)$$

of the ordinary quark condensate evaluated with respect to a phase $e^{i\varphi}$ in the temporal direction of the Euclidean theory. This phase is introduced by the generalized, $U(1)$ -valued boundary condition $\psi(\vec{x}, 1/T) = e^{i\varphi} \psi(\vec{x}, 0)$ in the temporal direction. For the usual antiperiodic boundary conditions for fermions we have $\varphi = \pi$, whereas $\varphi = 0$ corresponds to periodic boundary conditions. The φ -dependent quark condensate $\langle \bar{\psi}\psi \rangle_\varphi$ is proportional to

a sum over closed loops winding n -times around the compact time direction:

$$\langle \bar{\psi}\psi \rangle_\varphi = \sum_{l \in \mathcal{L}} \frac{e^{i\varphi n(l)}}{(am)^{|l|}} U(l). \quad (2)$$

Here \mathcal{L} denotes the set of all closed loops l with length $|l|$ on a lattice with lattice spacing a . Furthermore m is the quark mass. $U(l)$ stands for the chain of link variables in a loop l multiplied with appropriate sign and normalization factors, see Ref. [12] for details. Each loop that closes around the temporal boundary picks up factors of $e^{\pm i\varphi}$ according to its winding number $n(l)$. The Fourier transform in (1) projects out those loops with winding number n . The dual condensate Σ_1 then corresponds to loops that wind exactly once and is called the 'dressed Polyakov loop' [12]. This quantity transforms under center transformation identically as the conventional Polyakov loop [1] and is therefore an order parameter for center symmetry. The numerical agreement between dressed and conventional Polyakov loop has been established for gauge groups $SU(3)$ [13] and, remarkably, also for the centerless $G(2)$ [14].

These lattice calculations have been carried out in quenched QCD and in a formulation where the nontrivial $U(1)$ -valued boundary conditions are introduced for the measured operators only. Such a formulation avoids the complications associated with the introduction of nontrivial boundary conditions into the generating functional of QCD with fermions. The latter option is formally equivalent to the introduction of an imaginary chemical potential leading to the pattern of Roberge-Weiss periodicity of the generating functional [20]. In this work we will approximate the quenched lattice formulation and therefore do not encounter the Roberge-Weiss symmetry. A different approach is followed, however, in the (unquenched) renormalization group framework of Ref. [19], where the Roberge-Weiss symmetry is explicitly taken into account.

Furthermore, a comment on regularization is in order here. Below we will determine the dual condensate Σ_1 from Dyson-Schwinger equations in the infinite volume and continuum limit. For non-vanishing quark masses the quark condensate is quadratically divergent and needs to be properly regularized, see e.g. Ref. [21] for a recent discussion. Correspondingly, the loop expansion Eq. (2) breaks down for $a \rightarrow 0$. In this work we will employ an ultraviolet regulator in the form of a simple cutoff. For large enough cutoffs the regulator dependent part of the condensate is independent of temperature and therefore does not affect the chiral transition temperature. The regulator dependent part of the condensate is also independent of the boundary angle. Consequently it does not appear in the dual condensate and does not affect the deconfinement transition temperature T_{dec} either. The latter property can also be demonstrated *a posteriori* by comparing T_{dec} from the dual condensate with the one obtained from the dual scalar quark dressing function introduced in the next subsection. Since

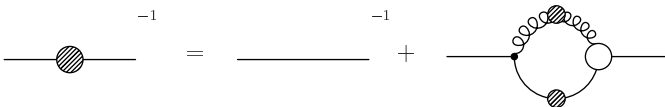


FIG. 1: The Dyson-Schwinger equation for the quark propagator. Filled circles denote dressed propagators whereas the empty circle stands for the dressed quark-gluon vertex.

the (dual) scalar quark dressing function does not suffer from regularization problems, agreement between the corresponding transition temperatures indicates that our regularization procedure is adequate. This is indeed the case as demonstrated in section IV C.

B. The dual scalar quark dressing function

Another order parameter for the deconfinement transition is the phase-Fourier-transform of the scalar quark dressing function evaluated at lowest Matsubara frequency and zero momentum. To derive this quantity note first that in momentum space the $U(1)$ -valued boundary conditions introduced above result in Matsubara modes $\omega_p(n_t, \varphi) = (2\pi T)(n_t + \varphi/2\pi)$ in the p_4 -direction, which depend on the boundary angle $\varphi \in [0, 2\pi[$. The inverse quark propagator can then be written as

$$S^{-1}(\vec{p}, \omega_p) = i\gamma_4 \omega_p C(\vec{p}, \omega_p) + i\gamma_i p_i A(\vec{p}, \omega_p) + B(\vec{p}, \omega_p), \quad (3)$$

with vector and scalar quark dressing functions C, A, B . A further tensor component proportional to $\sigma_{\mu\nu}$ is possible in principle but can be omitted in all practical calculations [22].

The scalar quark dressing function $B(\vec{p}, \omega_p)$ evaluated at $\vec{p} = 0$ and $\omega_p(0, \pi) = \pi T$ is an order parameter for the chiral phase transition in the chiral limit. It also serves as indicator for the chiral crossover at non-vanishing bare quark masses in a similar way as the chiral condensate does. Its dual

$$\Sigma_B = \int_0^{2\pi} \frac{d\varphi}{2\pi} e^{-i\varphi} B(0, \omega_p(0, \varphi)), \quad (4)$$

is an order parameter for the confinement-deconfinement transition. This can be shown in a similar fashion as for the spectral sums discussed in [11]: Using $B(0, \omega_p(0, \varphi)) = 1/4 \text{tr}[S^{-1}(0, \omega_p(0, \varphi))]$ we have

$$\Sigma_B = \int_0^{2\pi} \frac{d\varphi}{8\pi} e^{-i\varphi} \int d^3x \int_0^{1/T} dx_0 \text{tr}\langle \vec{x}, x_0 | D_\varphi^{-1} | 0 \rangle^{-1} \quad (5)$$

where D_φ is the (massive or chiral) Dirac operator evaluated under presence of the $U(1)$ -valued boundary conditions. A center transformation on Σ_B introduces an additional phase factor $z = e^{i2\pi k/N}$ with $k = 0, \dots, N_c - 1$ for N_c colors, which adds to the phase $e^{i\varphi}$ for our $U(1)$ -valued boundary conditions. We then obtain

$$\begin{aligned} z \Sigma_B &= \int_0^{2\pi} \frac{d\varphi}{8\pi} e^{-i\varphi} \int d^3x \int_0^{1/T} dx_0 \text{tr}\langle \vec{x}, x_0 | D_{\varphi+2\pi k/N}^{-1} | 0 \rangle^{-1} \\ &= z \int_0^{2\pi} \frac{d\varphi}{8\pi} e^{-i\varphi} \int d^3x \int_0^{1/T} dx_0 \text{tr}\langle \vec{x}, x_0 | D_\varphi^{-1} | 0 \rangle^{-1}, \end{aligned} \quad (6)$$

i.e. the dual scalar quark dressing Σ_B transforms under center transformations exactly like the conventional Polyakov loop and therefore acts as order parameter for the deconfinement transition in the heavy quark limit. This will be confirmed by our numerical results given below.

III. DYSON-SCHWINGER EQUATIONS FOR THE QUARK PROPAGATOR

A. The truncation scheme

The Dyson-Schwinger equation for the quark propagator Eq. (3) is displayed diagrammatically in Fig. 1. At finite temperature T it is given by

$$S^{-1}(\vec{p}, \omega_p) = Z_2 S_0^{-1}(\vec{p}, \omega_p) - C_F \frac{Z_2 \tilde{Z}_1}{\tilde{Z}_3} g^2 T \sum_{n_k} \int \frac{d^3k}{(2\pi)^3} \gamma_\mu S(\vec{k}, \omega_k) \Gamma_\nu(\vec{k}, \omega_k, \vec{p}, \omega_p) D_{\mu\nu}(\vec{p} - \vec{k}, \omega_p - \omega_k). \quad (7)$$

Here $D_{\mu\nu}$ denotes the (transverse) gluon propagator in Landau gauge and we have introduced a reduced quark-gluon vertex Γ_ν , by defining $\Gamma_{\nu,i}^{full} = ig \frac{\lambda_i}{2} \Gamma_\nu$. The bare quark propagator is given by $S_0^{-1}(p) = i\gamma \cdot p + Z_m m(\mu^2)$, where $m(\mu^2)$ is the renormalized current quark mass.

The Casimir factor $C_F = (N_c^2 - 1)/N_c$ stems from the color trace; in this work we only consider the gauge group $SU(2)$. The wave function and quark mass renormalization factors, Z_2 and Z_m , are determined in the renormalization process. The ghost renormalization factor \tilde{Z}_3

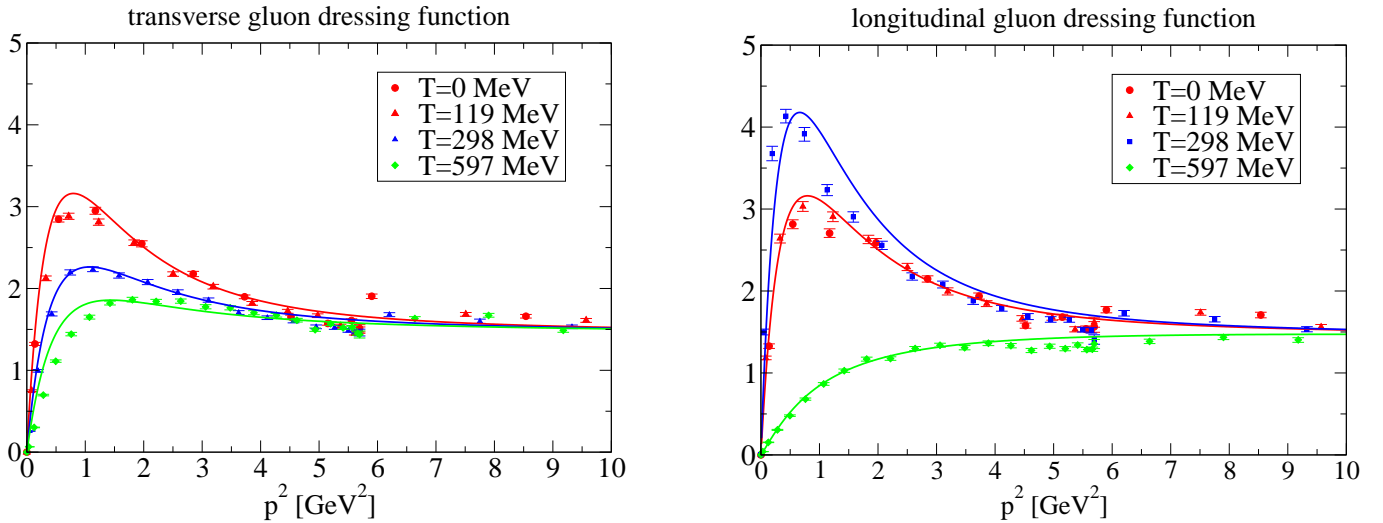


FIG. 2: Quenched $SU(2)$ lattice results for the transverse dressing function $Z_T(q)$ and the longitudinal dressing function $Z_L(q)$ of the gluon propagator [17] together with the fit functions Eq. (10). Note that the ultraviolet part of the lattice data has not been corrected for hyper-cubic artefacts; the fits (straight lines; see text) are adapted to the corresponding corrected data [25] at temperature $T = 0$.

is canceled by a corresponding factor in our model for the quark-gluon vertex discussed below. Furthermore we used $\tilde{Z}_1 = 1$ for the renormalization factor of the Landau gauge ghost-gluon vertex. The quark dressing functions $A(\vec{p}, \omega_p)$, $B(\vec{p}, \omega_p)$ and $C(\vec{p}, \omega_p)$ can be extracted from Eq. (7) by suitable projections in Dirac-space.

In order to solve this equation we have to specify explicit expressions for the gluon propagator and the quark-gluon vertex. At finite temperatures the tensor structure of the Landau gauge gluon propagator contains two parts, one transversal and one longitudinal to the heat bath. The propagator is then given by $(q = (\vec{q}, \omega_q))$

$$D_{\mu\nu}(q) = \frac{Z_T(q)}{q^2} P_{\mu\nu}^T(q) + \frac{Z_L(q)}{q^2} P_{\mu\nu}^L(q) \quad (8)$$

with transverse and longitudinal projectors

$$\begin{aligned} P_{\mu\nu}^T(q) &= \left(\delta_{ij} - \frac{q_i q_j}{\vec{q}^2} \right) \delta_{i\mu} \delta_{j\nu}, \\ P_{\mu\nu}^L(q) &= P_{\mu\nu}(q) - P_{\mu\nu}^T(q), \end{aligned} \quad (9)$$

with $(i, j = 1 \dots 3)$. The transverse dressing $Z_T(\vec{q}, \omega_q)$ is also known as magnetic dressing function of the gluon, whereas the longitudinal component $Z_L(q)$ is called electric dressing function of the gluon propagator. At zero temperatures Euclidean $O(4)$ -invariance requires both dressing functions to agree, i.e. $Z_T(q) = Z_L(q) = Z(q)$.

For the momentum range relevant for Eq. (7) we nowadays have very accurate solutions for the gluon dressing function $Z(q)$ at zero temperature from both, lattice calculations and functional methods, see e.g. [23] and references therein. The temperature dependence of the gluon propagator, however, is much less explored, see e.g. [24]. In [17] a combined study on the lattice and

from Dyson-Schwinger equations records a very different temperature dependence of the electric and magnetic parts. This is shown in Fig. 2. The temperature effects on both the magnetic and electric dressing functions are such that there are almost no effects when comparing the $T = 0$ result with $T = 119$ MeV. Further increasing the temperature to $T = 298$ MeV and $T = 597$ MeV significantly decreases the bump in the magnetic dressing function around $p^2 = 1$ GeV². There is no indication that this decrease takes special notice of the critical temperature $T_c \approx 300$ MeV for quenched QCD with gauge group $SU(2)$. The opposite seems to be true for the electric part of the propagator. Here from $T = 119$ MeV to $T = 300$ MeV one observes a clear increase of the bump in the dressing function $Z_L(q)$ and a subsequent decrease when the temperature is further raised to $T = 597$ MeV. Pending further investigation it seems reasonable to assume that the maximum of the bump is reached at or around the critical temperature $T_c \approx 300$ MeV.

Although the lattice data still have considerable systematic errors [17] they may very well correctly represent the qualitative temperature dependence of the gluon propagator. We therefore use a temperature dependent (qualitative) fit to the data as input into the DSE; this fit is also displayed in Fig. 2 (straight lines). Note that for momenta around $p^2 = 6$ GeV² the lattice data show considerable systematic errors due to hyper-cubic artefacts.

T[MeV]	0	119	298	597
$a_T(T)$	1	1	1.34	1.65
$a_L(L)$	1	1	0.8	4.0

TABLE I: Temperature dependent fit parameter of Eq.(10).

For the fits we have eliminated these artefacts by comparison with the $T = 0$ lattice result of Ref. [25], where these errors have been corrected. The fit functions read

$$Z_{T,L}(\vec{q}, \omega_q, T) = \frac{q^2 \Lambda^2}{(q^2 + \Lambda^2)^2} \left\{ \left(\frac{c}{q^2 + \Lambda^2 a_{T,L}(T)} \right)^2 + \frac{q^2}{\Lambda^2} \left(\frac{\beta_0 \alpha(\mu) \ln[q^2/\Lambda^2 + 1]}{4\pi} \right)^\gamma \right\}, \quad (10)$$

with the temperature independent scale $\Lambda = 1.4$ GeV and the coefficient $c = 9.8$ GeV². For gauge group $SU(2)$ we have $\beta_0 = 22/3$ and $\gamma = -13/22$ in the quenched theory and we renormalize at $\alpha(\mu) = 0.3$. The temperature de-

pendent scale modification parameters $a_{T,L}(T)$ are given in table I. In order to extend this fit to temperatures not given in the table we assume $a_{T,L}(T)$ to be temperature independent below $T = 119$ MeV and only slowly rising above $T = 597$ MeV. For $T \in [119, 597]$ MeV we use cubic splines to interpolate smoothly between the values given in table I. We expect the systematic error of this procedure to be of the same order as the systematic errors inherent in the lattice data. We also inherit the scale determined on the lattice using the string tension $\sqrt{\sigma} = 0.44$ GeV [17].

For the quark-gluon vertex with gluon momentum $q = (\vec{q}, \omega_q)$ and the quark momenta $p = (\vec{p}, \omega_p), k = (\vec{k}, \omega_k)$ we employ the following temperature dependent model

$$\Gamma_\nu(q, k, p) = \tilde{Z}_3 \left(\delta_{4\nu} \gamma_4 \frac{C(k) + C(p)}{2} + \delta_{j\nu} \gamma_j \frac{A(k) + A(p)}{2} \right) \left(\frac{d_1}{d_2 + q^2} + \frac{q^2}{\Lambda^2 + q^2} \left(\frac{\beta_0 \alpha(\mu) \ln[q^2/\Lambda^2 + 1]}{4\pi} \right)^{2\delta} \right), \quad (11)$$

where $\delta = -9/44$ is the anomalous dimension of the vertex. Note that because of $\gamma + 2\delta = -1$ the gluon dressing function together with the quark-gluon vertex behaves like the running coupling at large momenta; this is a necessary boundary condition for any model interaction in the quark DSE. The dependence of the vertex on the quark dressing functions A and C is motivated by the Slavnov-Taylor identity for the vertex; it represents the first term of a generalization of the Ball-Chiu vertex [26] to finite temperatures. The remaining fit function is purely phenomenological, see e.g. [27] where an elaborate version of such an ansatz has been used to describe meson observables. Here we use $d_1 = 7.6$ GeV² and $d_2 = 0.5$ GeV². A moderate variation of these parameters shifts the critical temperatures of both, the chiral and the deconfinement transition but leaves all qualitative aspects of the results presented below unchanged.

To our knowledge the truncation scheme defined above is the first of its kind within the DSE-approach that implements a realistic temperature dependence of the gluon propagator and the quark-gluon vertex beyond simple ansätze, see e.g. [22, 28, 29, 30] for previous approaches. The explicit expressions of the resulting DSEs for the quark dressing functions including Eq. (10) and Eq. (11) are given in appendix A. Unless explicitly denoted otherwise all results presented in section IV of this work are obtained using these DSEs.

For the sake of comparison, however, we also employed a simplified input, where all temperature dependencies are solely due to the quark propagator. To this end we fix the temperature dependent parameter $a_{T,L}(T)$ in the gluon dressing function to their zero temperature values and remove the temperature effects in the vertex using

$$\Gamma_\nu(q, k, p) = \tilde{Z}_3 \gamma_\nu \left(\frac{d_1}{d_2 + q^2} + \frac{q^2}{\Lambda^2 + q^2} \left(\frac{\beta_0 \alpha(\mu) \ln[q^2/\Lambda^2 + 1]}{4\pi} \right)^{2\delta} \right). \quad (12)$$

with (modified) fit parameters $d_1 = 10$ GeV² and $d_2 = 0.2$ GeV² such that the chiral transition temperature is the same as for the temperature dependent interaction.

Finally, when investigating the effect of the details of the quark-gluon interaction on the phase transition an interesting question concerns the influence of the deep infrared behavior of the ghost and gluon propagators as

well as the quark-gluon vertex on the phase transition. To this end we note that the expressions (10) and (11) for the gluon propagator and the quark-gluon vertex employed above correspond to decoupling type of infrared behavior in the sense specified in [23]. The corresponding expressions for scaling in the infrared are given in appendix C, where also corresponding numerical results

for the temperature dependent condensates are given. As a result we find that the chiral and deconfinement transitions is insensitive to the question of scaling vs. decoupling in the deep infrared.

B. Numerical procedure

Infinite volume/continuum DSEs:

The numerical solutions of the DSE are found using the conventional fixed point iteration method. The loop integral and Matsubara sum is regularized using a sharp cutoff $\Lambda = \sqrt{5} \times 10^2$ GeV such that the integration and summation extends to momenta and frequencies with $\omega_q^2 + \vec{q}^2 \leq \Lambda^2$. This is requisite to restore $O(4)$ invariance at perturbative momenta as well as in the limit of zero temperature. We apply a MOM renormalization scheme which defines the renormalization constants in such a way as to fix the full propagator at a certain momentum. We explicitly verified that the resulting renormalized quark propagator is independent of the size of the ultraviolet cutoff by increasing/decreasing the cutoff by an order of magnitude. The renormalized quark mass $m(\mu)$ has contributions stemming from the explicit chiral symmetry breaking and from the quark condensate. Since the quark condensate is temperature dependent fixing the renormalized quark mass with temperature independent renormalization conditions means that the magnitude of explicit chiral symmetry breaking changes with temperature. In order to minimize this effect we choose a very large renormalization point such that the quark condensate term is irrelevant there and the temperature effects in $m(\mu)$ can safely be ignored. The renormalization conditions are $C(\mu) = 1$ and $B(\mu) = m(\mu)$ with $\mu = (\vec{\mu}, \pi T)$ and $\vec{\mu}^2 = 10545$ GeV². The choice $m(\mu) = 1.85$ MeV then matches the renormalization conditions in Ref. [16] for mass 10 MeV at $T = 200$ MeV and $\vec{\mu}^2 = 20$ GeV² and corresponds roughly to an up quark mass. For $|n_t| \leq 20$ the summation over Matsubara frequencies is performed explicitly. The remaining sum is approximated by an integral that can be done with standard Gauss-Legendre integration.

In the chiral limit the transition temperature for the chiral phase transition is unambiguously defined by the temperature at which the symmetry is completely restored. This is signaled by the vanishing of the order parameters i.e. the quark mass function at zero momentum or equivalently the vanishing of the chiral quark condensate. For explicitly broken chiral symmetry we encounter a crossover rather than a phase transition and the transition temperature may depend on its definition. It can be defined by the peak of the chiral susceptibility

$$\chi = \partial/(\partial m) \langle \bar{\psi}\psi \rangle \quad (13)$$

or the renormalized chiral susceptibility

$$\chi_R = m^2 \frac{\partial}{\partial m} \left(\langle \bar{\psi}\psi \rangle_T - \langle \bar{\psi}\psi \rangle_{T=0} \right) \quad (14)$$

which can be made dimensionless by normalizing with T^4 for details see Refs. [2, 3]. An alternative definition of the transition temperature is via the (normalized) slope of the condensate with temperature

$$\tau = \sup_T \left(- \frac{\partial \langle \bar{\psi}\psi \rangle}{T^2 \partial T} \right). \quad (15)$$

The φ dependent quark condensate is determined according to

$$\langle \bar{\psi}\psi \rangle_\varphi = Z_2 N_c T \sum_{\omega_p(\varphi)} \int \frac{d^3 p}{(2\pi)^3} \text{tr}_D S(\vec{p}, \omega_p(\varphi)) \quad (16)$$

with the conventional quark condensate obtained for $\varphi = \pi$ and multiplication with Z_m . As mentioned in section II A, the integral in (16) is divergent for nonzero quark masses and needs to be regularized. To this end we introduce a cutoff at large enough momenta where the quark propagator in the integrand is temperature independent to very good approximation. The resulting regularized condensate is not indicative as concerns its absolute value but retains its correct dependence on temperature T and boundary angle φ as long as the temperature is much smaller than the cutoff scale. This is the case for all results presented in the following.

DSEs on a torus:

In Ref. [16] first results for the ordinary and the dual chiral condensate have been presented in a formulation of the Dyson-Schwinger equations on a torus. Such a formulation has the advantage of considerable simplifications as concerns the numerics but has the disadvantage of introducing artefacts due to the finite volume and lattice spacing. The calculations on a torus have been carried out at a three-volume of $V = (5 \text{ fm})^3$. This is sufficiently large to avoid significant volume effects even for quark masses as small as $m(\vec{\mu}^2 = 20 \text{ GeV}^2) = 10$ MeV used in Ref. [16]. For even larger volumes one obtains small changes of the order of a few percent in the chiral condensate below the critical temperature and much smaller effects for larger temperatures; the value of the chiral transition temperature is unaffected. In addition there are effects due to the finite lattice spacing in temporal and spatial directions and the fact that the renormalized quark mass $m = B(\pi T, \vec{\mu})/C(\pi T, \vec{\mu})$ has been treated as a constant with respect to variations in temperature [16]. This is certainly correct for a very large renormalization point $\vec{\mu}$, but introduces temperature dependent artefacts for the value $\vec{\mu}^2 = 20$ GeV used in the torus calculation. In this work we remove these artefacts by the following procedure: we first solve the Dyson-Schwinger equations in the infinite volume/continuum limit, i.e. in the formulation introduced in section III. These equations are renormalized at a very large renormalization point and consequently temperature effects in the renormalization procedure are absent. From these results we read off the corresponding, temperature dependent renormalization conditions at the small renormalization point $\vec{\mu}^2 = 20$ GeV² of our torus formulation. These are then

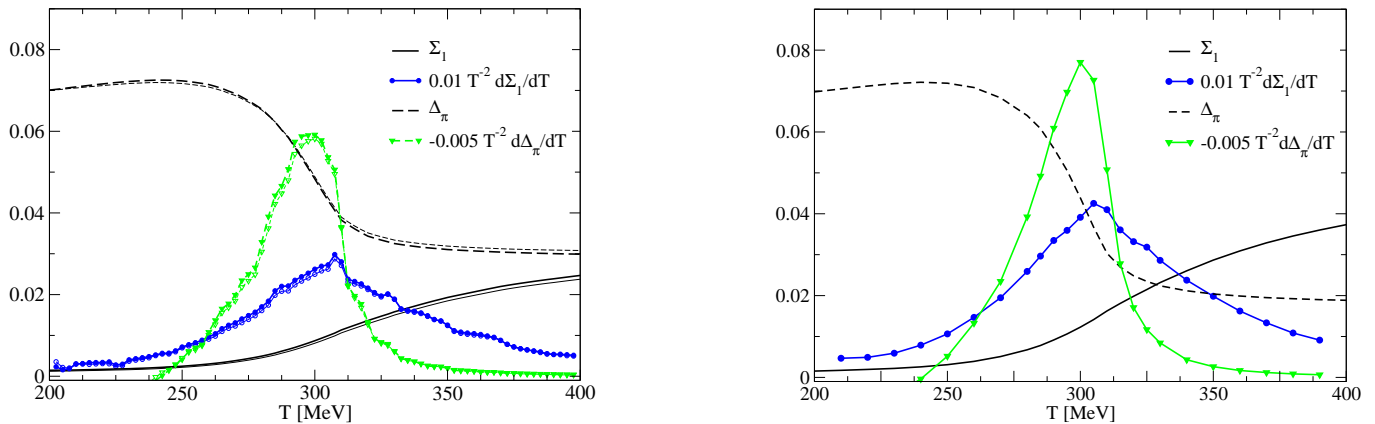


FIG. 3: Left diagram: Temperature dependence of the dressed Polyakov-loop Σ_1 and the conventional quark condensate $\Delta_\pi \equiv \langle \bar{\psi}\psi \rangle_{\varphi=\pi}$ together with their derivatives for $m = 10$ MeV evaluated at two different ultraviolet cutoffs (thick lines and filled symbols for the large cutoff; thin lines and open symbols for the smaller cutoff). Right diagram: The same calculation in the infinite volume limit and at an extremely large ultraviolet cutoff. Note that the ordinary condensates in both plots have been shifted to agree at $T = 200$ MeV.

applied to the calculations on the torus. This procedure is justified if and only if the truncation of the quark-DSE respects multiplicative renormalizability, which is the case for our truncation scheme. As we will see below, this change in the renormalization procedure leads to a significant change in the deconfinement transition temperature on the torus as compared to the one extracted in Ref. [16].

The numerical details for the calculation on a torus are similar to the ones in the zero temperature limit, discussed at length in Refs. [31]. As concerns corrections for hyper-cubic artefacts we employ the 'cutting-the edges' prescription developed in [31] in the three spatial directions of the torus. For the temporal direction we take into account as many Matsubara modes as necessary to arrive at approximately the same cutoff scale as for the spatial directions. This results e.g. in $n_t = 8$ temporal Matsubara modes at $T = 200$ MeV.

These prescriptions are adapted to minimize volume and discretization artefacts when comparing solutions from DSEs on a torus with the corresponding results in the infinite volume/continuum limit. At this point we do not claim that the remaining volume and spacing effects are similar to the corresponding ones in lattice calculations. Nevertheless it is interesting to investigate the details of the volume and cutoff-dependence of our torus results systematically. While first results of this comparison are presented in the next section, a more detailed analysis is deferred to future work.

IV. NUMERICAL RESULTS

A. The infinite volume and continuum limit

We first compare results from DSEs on a torus with results from the infinite volume/continuum DSEs at a

quark mass that roughly corresponds to an up-quark. The resulting temperature dependent ordinary and dual condensates as well as their (normalized) temperature derivatives are shown in Fig. 3. The left hand diagram displays the torus results at two different ultraviolet cutoffs $p_{max} = 5.96, 7.45$ GeV corresponding to lattice spacings of $a = \pi/p_{max} \approx 0.1, 0.08$ fm, respectively. The right hand diagram shows our results in the continuum. Compared to Ref. [16] we use a modified mass renormalization scheme on the torus as described in the last subsection. Furthermore we normalize the temperature derivatives with $1/T^2$ to obtain dimensionless quantities. The last change affects both transition temperatures only by 1-2 MeV. The effects of the modified mass renormalization procedure can be assessed by comparing our results with the ones shown in Fig. 3 of Ref. [16]. We obtain a more pronounced chiral transition with a narrower peak in the temperature derivative of the ordinary chiral condensate. The corresponding transition temperature $\tau \approx 300$ MeV is unchanged. As for the dual condensate, or dressed Polyakov loop, the peak of the temperature derivative is shifted to smaller temperatures, i.e. from $T_{dec} \approx 320$ MeV in Ref. [16] to our value $T_{dec} \approx 308$ MeV for both cutoffs. Despite this shift, the deconfinement transition remains separate from the chiral transition.

This finding is also visible in the infinite volume/continuum limit. Although there are still differences in the details of the temperature dependence of the ordinary and dual condensate between torus and continuum DSEs, the related peaks in the temperature derivatives are similar; here we find $\tau \approx 301$ MeV and $T_{dec} \approx 308$ MeV, i.e. still (slightly) different transition temperatures. This gap reduces further when the corresponding transition temperatures from the chiral susceptibilities χ_R/T^4 and χ_R are considered, see table II.

In general, our results in the infinite volume/continuum limit agree qualitatively with the

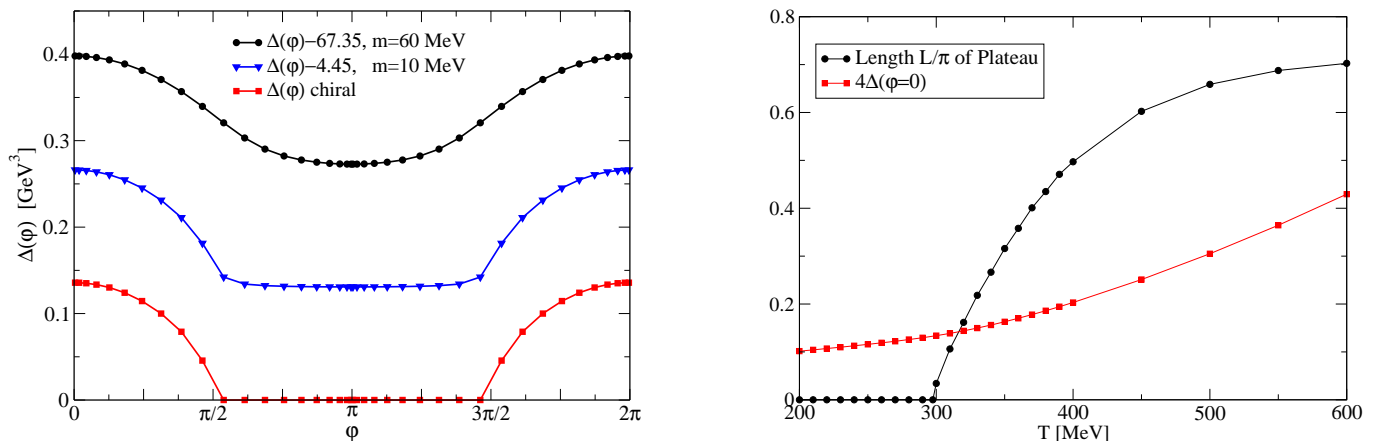


FIG. 4: Left diagram: Angular dependence of the quark condensate evaluated at two different quark masses and in the chiral limit at $T = 400$ MeV. Right diagram: Temperature dependence of the half-width L of the plateau in the chiral quark condensate in units of π (i.e. $L/\pi = 1$ means that the plateau extends over all angles $\varphi = 0 \dots 2\pi$) and temperature dependence of the chiral quark condensate $\Delta(\varphi)$ at periodic boundary conditions $\varphi = 0$.

ones on a torus and almost quantitatively as concerns the transition temperatures. The most prominent remaining discrepancy is seen in the relative decrease of the ordinary condensate and the relative increase of the dual condensate below and above the transition temperature. This difference is a cutoff effect, as can be inferred from comparing results for the two different lattice spacings in the left plot of Fig. 3. In particular we found that cutoff effects in the quark-DSE only play a very minor role, whereas the cutoff effects in the condensate equation (16) are most significant. These effects will be explored further in future work.

In general we wish to emphasize that the present calculation, although carried out with quenched lattice results for the gluon propagator, is in itself not strictly quenched: our ansatz for the quark-gluon vertex is too simple to strictly represent the quenched theory. This can be seen from the fact that the dressed Polyakov-loop is not strictly zero below the deconfinement transition. Consequently we do not observe the second order deconfinement phase transition expected from quenched $SU(2)$ Yang-Mills theory but a, more or less rapid, crossover at $T_{dec} \approx 308$ MeV¹. On the other hand, as concerns the

τ	T_{χ_R}/T^4	T_{χ_R}	T_{dec}
301(2)	304(1)	305(1)	308(2)

TABLE II: Transition temperatures in the infinite volume/continuum limit for the different definitions Eqs. (13), (14) and (15). These values have been extracted from numerical results evaluated using temperature steps of one MeV (not shown in Fig.3).

chiral properties of our model, a prominent feature of the quenched theory not reproduced by our framework is the appearance of quenched chiral logarithms in the chiral condensate. These are well-known to be generated by η' hairpin diagrams, which are not represented by our vertex ansatz. For the present investigation this is more an advantage than a drawback. Quenched chiral logarithms are most notable in the chiral limit, where they lead to a singularity in the chiral condensate. Since we do not encounter this singularity we are in a position to investigate both, the ordinary and the dual condensate in the chiral limit.

B. The chiral limit

In Fig. 4 we study the dependence of the quark condensate on the boundary angle φ . In the left diagram we compare the angular dependence of the condensate at $T = 400$ MeV for two different quark masses and in the chiral limit. As already noted in Ref. [16] we clearly see a broadening in the central dip of the graphs with decreasing quark mass. This can be readily understood from the loop expansion of the quark condensate, Eq. (2), which is applicable at finite quark masses and under presence of an ultraviolet regulator for the condensate, cf. section III B. At sufficiently large quark masses large loops are suppressed by powers of $1/m$. As a result only loops winding once around the torus should contribute in Eq. (2) and the resulting angular behavior of the condensate should be proportional to $\cos(\varphi)$. Indeed, this is what we see: the result for our largest quark

¹ Note that even if our vertex were strictly quenched it is not clear whether the lattice input for the gluon propagator is precise

enough to allow for an observation of the second order phase transition expected in $SU(2)$ Yang-Mills theory

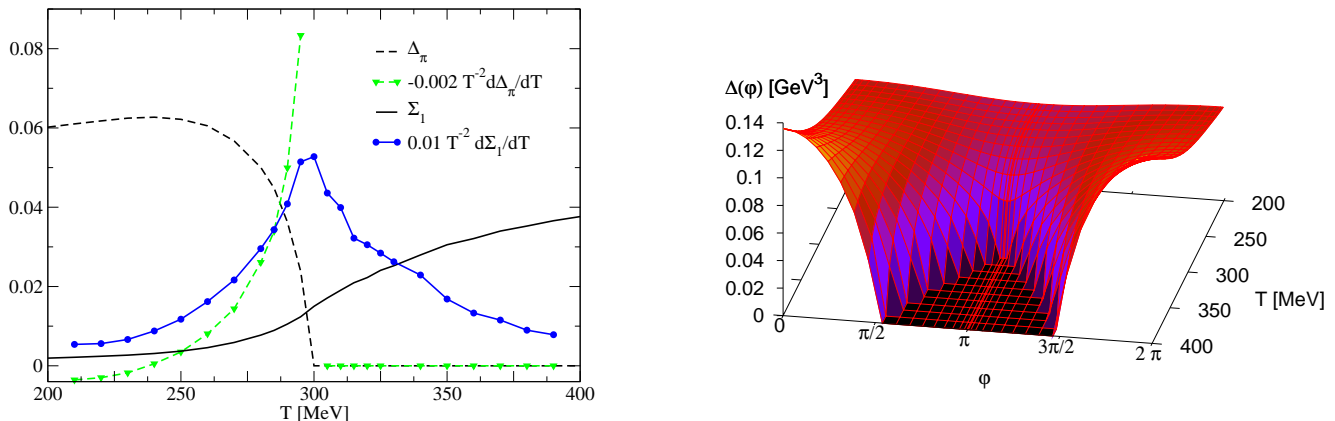


FIG. 5: Left diagram: Temperature dependence of the conventional and dual condensates as well as their temperature derivatives in the chiral limit. Right diagram: A 3d-plot of the angular and temperature dependence of the chiral quark condensate.

mass can well be fitted by only few terms in an expansion $\Delta(\varphi) = \sum_{n=0}^N a_n \cos(n\varphi)$ and the first term is by far the largest contribution. For smaller quark masses we observe also sizeable contributions from terms $\cos(n\varphi)$ with $n > 1$. In the plot, these contributions are responsible for the flat area around the antiperiodic boundary angle $\varphi = \pi$. Approaching the chiral limit this area becomes flatter and finally develops a derivative discontinuity at two finite values of $\varphi = \pi \pm L$. These indicate the breakdown of the loop expansion Eq. (2) in the chiral limit. Note that this is also the limit where the condensate is free of quadratic ultraviolet divergencies and the continuum limit can be taken; another reason why the loop expansion Eq. (2) is no longer applicable.

In the plot on the right hand side of Fig. 4 we show the temperature dependence of the half-width L of the plateau in the chiral quark condensate in units of π . The width of the plateau is zero below the critical temperature T_c and rises quickly above, spreading up to $L/\pi = 0.6$ for temperatures in the region $T \approx 2T_c$. This monotonic rise then slows down considerably and seems to converge to a finite value smaller than one. However, from the presently available results up to $T \approx 2.5T_c$ one cannot completely exclude that the plateau finally extends over the whole range of boundary angles $\varphi = 0 \dots 2\pi$ for $T \rightarrow \infty$.

The behavior of the chiral quark condensate at periodic boundary conditions, $\Delta(\varphi = 0)$, is also a monotonic function of temperature as shown in the same plot. From a naive dimensional analysis of the condensate one may expect that it rises proportional to the third power of the temperature. This is however not correct as explicitly shown in our analytical analysis in appendix B. There we demonstrate that

$$\Delta_{\varphi=0}(T) \sim T^2 \quad \text{for } T \gg T_c. \quad (17)$$

To extract this behavior also from our numerical data

we fitted a polynomial of degree three in T : the result, $\Delta_{\varphi=0}(T \gg T_c) = 10^{-5} + 0.045(1)T + 0.73(1)T^2 + 10^{-7}T^3$, for temperatures $T > 2T_c$ clearly agrees with the analytical analysis. This scaling behavior also agrees with corresponding results of Ref. [19]. In addition it may be interesting to note that this T^2 -scaling of the condensate at periodic boundary conditions agrees with the naive scaling of the chiral condensate of the resulting three-dimensional theory in the infinite temperature limit.

In the diagram of the left hand side of Fig. 5 we plot the temperature dependence of the ordinary and the chiral condensate as well as their temperature derivatives in the chiral limit. One clearly observes a second order chiral phase transition. The temperature derivative of the ordinary condensate diverges at the corresponding critical temperature $T_c = \tau = T_{\chi_R}/T^4 = 298(1)$ MeV. Above T_c the ordinary condensate is strictly zero. For the deconfinement transition we observe a qualitatively similar behavior as for the case with finite quark mass discussed in the last subsection. The corresponding transition temperature, however, has moved to a lower value, $T_{dec} = 299(3)$ MeV, and coincides almost precisely with the chiral critical temperature. This is in agreement with corresponding extrapolations within lattice QCD [32]. We regard this as one of the main results of the present investigation.

A combined plot of the angular and temperature dependence of the chiral limit condensate is shown in the right hand diagram of Fig. 5. We clearly observe a different evolution of the quark condensate at different boundary angles φ . Whereas at periodic boundary conditions $\varphi = 0, 2\pi$ the condensate is monotonically rising, cf. the curve in the right diagram in Fig. 4, it clearly shows signals for a phase transition for boundary angles close to antiperiodic boundary conditions $\varphi = \pi$, cf. the corresponding curve in the left diagram of Fig. 5. Indeed for angles around $\varphi = \pi$ one could (formally) define a φ -

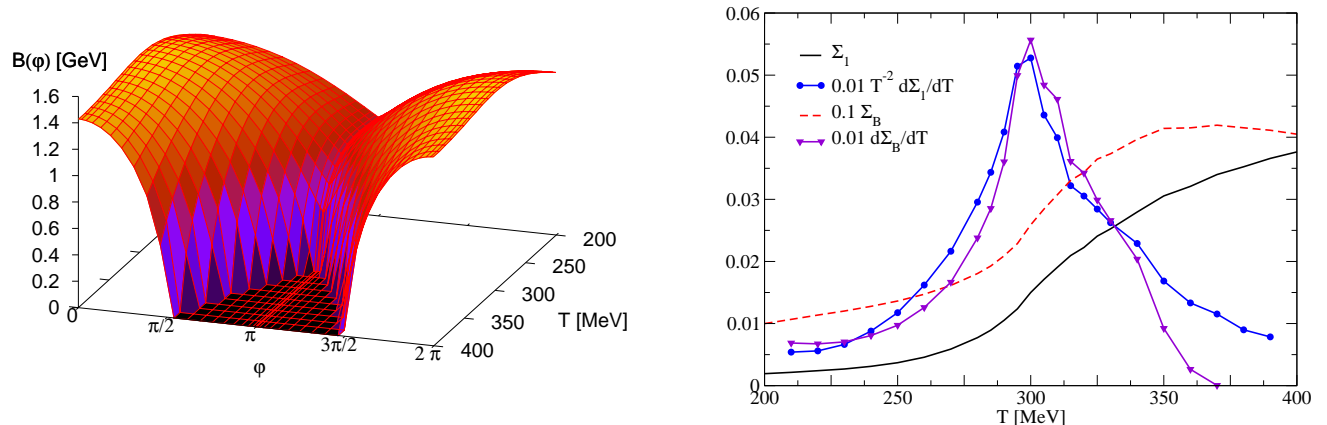


FIG. 6: Left diagram: A 3d-plot of the angular and temperature dependence of the quark scalar dressing function evaluated at zero momentum and lowest Matsubara frequency. Note that for $T > 400$ MeV (not shown in the plot) the scalar quark dressing function at periodic boundary conditions starts to rise linearly with temperature, $B_{\varphi=0,p=0}(T) \sim T$. Right diagram: Comparison of the temperature dependence of the corresponding dual scalar quark dressing and the dual condensate.

dependent transition temperature that is related to the width L of the plateau.

Finally we would like to make two comments. First, the corresponding dependence of the massive quark condensate as function of (T, φ) is similar to that of its chiral counterpart. The most pronounced difference is that there is no plateau around $\varphi = \pi$, but instead a cosine-shaped dip as can be inferred from the left diagram in Fig. 4. Second, we also determined the chiral condensate using the simplified, temperature independent quark-gluon interaction, Eq. (12), and a gluon propagator fixed at $T = 0$. This form of the interaction allows for temperature effects in the quark propagator only, while retaining the chiral critical temperature $\tau \approx 300$ MeV. The corresponding result is qualitatively similar to the one with full temperature dependence in the interaction. However, both transitions are much less pronounced. The chiral condensate starts to decrease and the dual condensate starts to increase at much lower temperatures. Correspondingly we obtain broad curves for the temperature derivatives. We conclude that a quantitative study of the details of the phase transitions of QCD has to take into account the temperature effects in the interaction.

C. The dual scalar quark dressing function

We now come back to the dual scalar quark dressing introduced by Eq. (5). Our numerical results for the angular and temperature dependence of the scalar quark dressing function $B(0)$ is shown in the left diagram of Fig. 6. The resulting pattern is similar to the one for the quark condensate, cf. Fig. 5, in particular as concerns the opening of a zero plateau around antiperiodic

boundary conditions above the critical temperature. For temperatures below T_c we observe a more distinct φ dependence as for the dual condensate, again indicating the non-quenched nature of our model for the quark-gluon vertex as discussed above. Above T_c the scalar quark dressing function $B_{\varphi=0}(0)$ at periodic boundary conditions stays constant for a while but then starts to rise for temperatures above $2T_c$ (not shown in the 3d-plot). Our fit to the data leaves us with

$$B_{\varphi=0,p=0}(T) \sim \sqrt{T} \quad \text{for } T \gg T_c \quad (18)$$

in agreement with our analytical analysis in appendix B and corresponding results of Ref. [19].

The data for the dual scalar quark dressing are shown on the right hand diagram of Fig. 6 and compared to the dual condensate. Again, the temperature dependence of both quantities is very similar. The temperature derivatives clearly peak at precisely the same transition temperature, indicating the deconfinement transition. Also, the rate of change at and around the transition temperature is quantitatively similar, although the signal is slightly stronger for the dual scalar dressing function Σ_B . From a systematic perspective the dual condensate, or dressed Polyakov loop, has the advantage of a direct connection to the ordinary Polyakov loop in the limit of static quarks. However, the dual scalar quark dressing function has the advantage of being a well defined quantity in the continuum limit. After renormalization of the Dyson-Schwinger equation of the quark propagator this quantity stays finite when the cutoff is sent to infinity also for finite quark masses. Both quantities are promising candidates for a further study of the deconfinement transition of QCD.

V. SUMMARY AND CONCLUSIONS

In this work we have investigated the chiral and the deconfinement transition of quenched QCD. From the temperature dependent quark propagator we extracted the order parameter for the chiral transition, the quark condensate, and order parameters for the deconfinement transition, the dressed Polyakov loop and the dual scalar quark dressing. We determined the quark propagator from its Landau gauge Dyson-Schwinger equation in the imaginary time Matsubara formalism. We emphasize once more that our truncation scheme, introduced in Ref. [16], implements a realistic temperature dependence of the gluon propagator and takes into account temperature effects in the quark-gluon vertex. It therefore goes beyond the simple models used in previous works.

When comparing results from the infinite volume/continuum DSEs with corresponding ones on a torus we found interesting effects due to different renormalization prescriptions for the quark propagator: the deconfinement transition temperature on a torus is shifted to smaller temperatures, i.e. from $T_{dec} \approx 320$ MeV to $T_{dec} \approx 308$ MeV when artificial temperature effects in the renormalized quark mass are avoided. This value agrees precisely with $T_{dec} \approx 308(2)$ MeV in the infinite volume/continuum limit reflecting the fact that the remaining cutoff artefacts on our torus do not affect the transition temperature. The same is true for the chiral transition temperature. We find $\tau = 301(2)$ MeV from the temperature derivative of the chiral condensate and $T_{\chi_R/T^4} = 304(1)$ MeV from the normalized chiral susceptibility. In summary we conclude that the chiral and deconfinement transition temperatures are only slightly different for finite quark masses. This finding will be further tested in future work using more precise data for the gluon propagator.

In the chiral limit this agreement becomes exact (within numerical errors). We find a second order chiral phase transition at $T_c = 298(1)$ MeV and a similar temperature for the deconfinement transition, $T_{dec} = 299(3)$ MeV. It is worth to emphasize again that both transition temperatures are extracted from the properties of the quark propagator and therefore related to the underlying properties of the Dirac operator. Therefore in a sense discussed in more detail in Refs. [8, 9, 10, 11, 19] the chiral and the deconfinement transition are closely

connected.

The framework used in this work is quenched $SU(2)$ Yang-Mills theory. Our transition temperatures may be translated into the corresponding ones of quenched $SU(3)$ QCD using the relations $T_c/\sqrt{\sigma} = 0.709$ ($SU(2)$) and $T_c/\sqrt{\sigma} = 0.646$ ($SU(3)$) between the respective critical temperatures and the string tension [33]. The resulting transition temperatures are then $T_{\chi_R/T^4} \approx 277$ MeV and $T_{dec} \approx 281$ MeV for the massive case and $T_{\chi_R/T^4} \approx T_{dec} \approx 272$ MeV in the chiral limit. In order to work in the full, unquenched theory we would have to take into account quark-loop effects in the gluon propagator and meson effects in the quark-gluon vertex [27]. These effects will shift the transition temperatures below $T = 200$ MeV, see [4, 5] for latest results for $N_f = 2 + 1$ quark flavors. As concerns the dual condensate and scalar dressing function in the unquenched formulation one needs to carefully take into account effects due to the Roberge-Weiss symmetry [20]. This is because of the formal similarity of the continuous boundary conditions for the quark field to an imaginary chemical potential, see [19] for details. An investigation of these effects as well as a detailed study of volume and discretization artefacts is deferred to future work.

Acknowledgments

We thank Falk Bruckmann, Christof Gattlinger, Erwin Laermann, Jan Pawłowski, Rob Pisarski, Lorenz von Smekal and Wolfgang Soeldner for discussions. We are grateful to Axel Maas for discussions and for making the lattice data of Ref. [17] available. This work has been supported by the Helmholtz Young Investigator Grant VH-NG-332 and by the Helmholtz Alliance HA216-TUD/EMMI.

APPENDIX A: EXPLICIT FORM OF THE DSEs FOR THE QUARK DRESSING FUNCTIONS

DSEs in the infinite volume/continuum limit:

The explicit form of the DSEs in the infinite volume/continuum limit in the truncation specified in section III A is given by

$$\begin{aligned}
A(k) = & Z_2 + \frac{Z_2 g^2}{\vec{k}^2} C_F T \sum_{n_q} \int \frac{d^3 q}{(2\pi)^3} \frac{1}{(\omega_q^2 C^2(q) + \vec{q}^2 A^2(q) + B^2(q))} \times \\
& \left\{ C(q) \Delta^L(p) \omega_q (\omega_q - \omega_k) \frac{\vec{q}^2 - \vec{p}^2 - \vec{k}^2}{p^2} \frac{\Gamma^C(q, k) + \Gamma^A(q, k)}{2} \right. \\
& + \frac{A(q)}{2} \left[\Delta^L(p) \frac{\vec{k}^2 + \vec{q}^2 - \vec{p}^2}{p^2} \left(\Gamma^C(q, k) \vec{p}^2 + \Gamma^A(q, k) \omega_p^2 \right) + \Delta^L(p) \frac{(\vec{q}^2 - \vec{k}^2)^2 - \vec{p}^4}{p^2} \Gamma^A(q, k) \right. \\
& \left. \left. + \left(\Delta^T(p) - \Delta^L(p) \right) \frac{(\vec{q}^2 - \vec{k}^2)^2 - \vec{p}^4}{\vec{p}^2} \Gamma^A(q, k) \right] \right\}, \tag{A1}
\end{aligned}$$

$$\begin{aligned}
B(k) = & Z_2 Z_m m + Z_2 g^2 C_F T \sum_{n_q} \int \frac{d^3 q}{(2\pi)^3} \frac{B(q)}{\omega_q^2 C^2(q) + \vec{q}^2 A^2(q) + B^2(q)} \times \\
& \left(\Delta^L(p) \frac{\omega_p^2 \Gamma^A(q, k) + \vec{p}^2 \Gamma^C(q, k)}{p^2} + 2 \Delta^T(p) \Gamma^A(q, k) \right), \tag{A2}
\end{aligned}$$

$$\begin{aligned}
C(k) = & Z_2 + \frac{Z_2 g^2}{\omega_k} C_F T \sum_{n_q} \int \frac{d^3 q}{(2\pi)^3} \frac{1}{\omega_q^2 C^2(q) + \vec{q}^2 A^2(q) + B^2(q)} \times \\
& \left(\omega_q C(q) \left[2 \Delta^T(p) \Gamma^A(q, k) + \Delta^L(p) \left(\Gamma^A(q, k) \frac{\omega_p^2}{p^2} - \Gamma^C(q, k) \frac{\vec{p}^2}{p^2} \right) \right] \right. \\
& \left. + \omega_p A(q) \Delta^L(p) \frac{\vec{p}^2 + \vec{q}^2 - \vec{k}^2}{2p^2} \left(\Gamma^C(q, k) + \Gamma^A(q, k) \right) \right) \tag{A3}
\end{aligned}$$

with $q = (\vec{q}, \omega_q)$, $k = (\vec{k}, \omega_k)$, $p = (\vec{p}, \omega_p) = q - k$, and the gluon propagator

$$\Delta^T(p) = \frac{Z_T(p)}{p^2}, \quad \Delta^L(p) = \frac{Z_L(p)}{p^2} \tag{A4}$$

and the vertex dressing functions

$$\Gamma^C(q, k) = \Gamma(q - k) \frac{C(q) + C(k)}{2} \quad \text{and} \quad \Gamma^A(q, k) = \Gamma(q - k) \frac{A(q) + A(k)}{2} \tag{A5}$$

with

$$\Gamma(q) = \left(\frac{d_1}{d_2 + q^2} + \frac{q^2}{\Lambda^2 + q^2} \left(\frac{\beta_0 \alpha(\mu) \ln[q^2/\Lambda^2 + 1]}{4\pi} \right)^{2\delta} \right). \tag{A6}$$

DSEs on a torus:

The corresponding form of the DSEs on a torus is similar to the one given in Eq. (A1), Eq. (A2) and Eq. (A3) with the exception that the three-dimensional momentum integral is replaced by a sum over momenta. In the three Cartesian spatial directions we thus have Matsubara sums counting momenta $\vec{p}_{\mathbf{n}} = \sum_{i=1..3} (2\pi/L)(n_i) \hat{e}_i$, where \hat{e}_i are Cartesian unit vectors in Euclidean momentum space. In [31] a technique of rearranging the three Cartesian sums into a sum over hyper-spheres and a sec-

ond sum over the individual momenta on each hyper-sphere has been developed that is convenient for the numerical treatment of the DSEs. This sum is given by

$$\frac{1}{L^3} \sum_{n_1, n_2, n_3} (\dots) = \frac{1}{L^3} \sum_{j, m} (\dots), \tag{A7}$$

where j counts spheres with $\vec{p}^2 = \text{const}$, and m numbers the grid points on a given sphere. The corresponding momentum vectors are denoted by $\vec{p}_{j, m}$.

APPENDIX B: LARGE TEMPERATURE SCALING OF $B_{\varphi=0}$ AND $\langle\bar{\psi}\psi\rangle_{\varphi=0}$

In this section we analyze the large temperature scaling of the scalar quark dressing function $B_{\varphi=0}(p, T)$ and the quark condensate $\langle\bar{\psi}\psi\rangle_{\varphi=0}(T)$ with temperature. To this end we first analyze the large temperature limit of the DSE Eq. (A2) for the scalar quark dressing function. With periodic boundary conditions $\varphi = 0$ only the zeroth Matsubara frequency $\omega_q = 0$ contributes in the Matsubara sum; all others are suppressed by powers of the temperature T . Furthermore at large enough temperatures the temperature effects in the gluon dressing functions and the vector dressing functions A and C of the quark propagator and quark-gluon vertex are arbitrary weak and therefore can be neglected. Working in the chiral limit we then have

$$\begin{aligned} B(\vec{k}, T) &\sim T \int \frac{d^3q}{(2\pi)^3} \frac{B(\vec{q}, T)}{\vec{q}^2 + B^2(\vec{q}, T)} \frac{3\Gamma(\vec{q} - \vec{k})}{(\vec{q} - \vec{k})^2} \\ &\sim T \int dq \frac{B(\vec{q}, T)}{\vec{q}^2 + B^2(\vec{q}, T)}. \end{aligned} \quad (\text{B1})$$

The second line follows from the first line because of the temperature independence of the terms in the angular integral. The resulting integral in Eq. (B1) is dominated from low momenta $\vec{q}^2 < B^2(\vec{q}, T)$ and consequently the integrand scales like $1/B(\vec{q}, T)$ leading to

$$B(\vec{k}, T) \sim \sqrt{T} \quad \text{for } T \gg T_c, \quad (\text{B2})$$

in agreement with our numerical results discussed in section IV C and corresponding results in Ref. [19]. We also confirmed that indeed the scaling of $B(\vec{k}, T)$ with T is independent of the three-momentum \vec{k} .

Having identified the large temperature scaling of $B(\vec{k}, T)$ we now analyze the integral for the quark condensate Eq. (16) given by

$$\begin{aligned} \langle\bar{\psi}\psi\rangle_{\varphi=0} &= 4 Z_2 N_c T \sum_{\omega_q} \int \frac{d^3q}{(2\pi)^3} \frac{B}{\omega_q^2 C^2 + \vec{q}^2 A^2 + B^2}, \\ &\sim T \int dq \vec{q}^2 \frac{B(\vec{q}, T)}{\vec{q}^2 + B^2(\vec{q}, T)} \end{aligned} \quad (\text{B3})$$

Here the second line is obtained by again neglecting the temperature scaling of the vector dressing functions A, C and the contributions of all but the lowest Matsubara frequency. The resulting integral has an extra factor of \vec{q}^2 as compared to the one in Eq. (B1). It is therefore not dominated by momenta smaller than B^2 . Recalling that $B(0, T) \sim B(\vec{q}, T) \sim \sqrt{T}$ we proceed by the integral transformation $q \rightarrow q' B(0, T)$ which leads to

$$\begin{aligned} \langle\bar{\psi}\psi\rangle_{\varphi=0} &\sim T \int dq' \vec{q}'^2 B^3(0, T) \times \\ &\quad \frac{B(\vec{q}, T)}{B^2(\vec{q}, T) \left(\vec{q}'^2 B^2(0, T) / B^2(\vec{q}, T) + 1 \right)}, \\ &\sim T^2, \quad \text{for } T \gg T_c. \end{aligned} \quad (\text{B4})$$

This result is again in excellent agreement with our numerical results discussed in section IV B.

APPENDIX C: SCALING VS. DECOUPLING

In this appendix we demonstrate that the deep infrared behavior of the gluon propagator and the quark-gluon vertex is not related to the details of the deconfinement transition at T_{dec} . The reason why we are interested in this question is an ongoing discussion over the past years on the status of two possible types of analytical infrared solutions of Yang-Mills theory. These two types of solutions are characterized by a one parameter family of boundary conditions on the dressing function of the ghost propagator, $G(p^2)$, at zero momentum. If $G(p^2 = 0) = \infty$ one observes the 'scaling' solution of infrared Yang-Mills theory, characterized by power laws in all one-particle irreducible Green's functions of the theory [34, 35, 36]. The other possibility, $G(p^2 = 0) < \infty$, describes 'decoupling' characterized by a finite gluon propagator and a finite ghost dressing function at zero momenta. [23, 37, 38]. Only the first of these two possibilities, scaling, is in agreement with the Kugo-Ojima criterion of well-defined global color charges [39, 40].

Nevertheless, both possibilities satisfy a confinement criterion developed in Ref. [18]: both types of infrared solutions lead to a confining Polyakov-loop potential. It has also been noted in Ref. [18] that the confinement-deconfinement phase transition extracted from the temperature dependence of the Polyakov-loop potential is not qualitatively affected by the choice of scaling or decoupling. Here we demonstrate that the same is true for the deconfinement transition from the dual quark condensate.

To this end we note that the choice of the fit-function Eq. (10) for the gluon propagator and the ansatz for the quark-gluon vertex Eq. (11) correspond to 'decoupling' in the deep infrared. An alternative choice that fits the lattice results of Ref. [17] for the temperature dependent gluon propagator equally well is given by

$$Z_T^{scaling}(\vec{q}, \omega_q, T) = Z_T(\vec{q}, \omega_q, T) \left(\frac{q^2}{q^2 + \Lambda_{IR}^2} \right)^{2\kappa+1/2-1} \quad (\text{C1})$$

$$Z_L^{scaling}(\vec{q}, \omega_q, T) = Z_L(\vec{q}, \omega_q, T), \quad (\text{C2})$$

where $Z_{T,L}(\vec{q}, \omega_q, T)$ are given by Eq. (10). The effect of the extra factor is to convert the infrared behavior $Z_T(\vec{q}, \omega_q, T) \sim q^2$ of the decoupling type of gluon dressing function to the scaling behavior $Z_T^{scaling}(\vec{q}, \omega_q, T) \sim (q^2)^{2\kappa+1/2}$ with the anomalous dimension $\kappa \approx 0.40$ [41] of the three-dimensional theory. Corresponding scaling solutions from DSEs have been reported in Ref. [17]. Note that the electric part of the gluon propagator always develops a screening mass and is therefore not modified in Eq. (C2). The scale Λ_{IR} is typically much smaller than Λ_{QCD} ; here we choose $\Lambda_{IR} = 100$ MeV in agreement with the results of [23]. The scaling of the quark-gluon

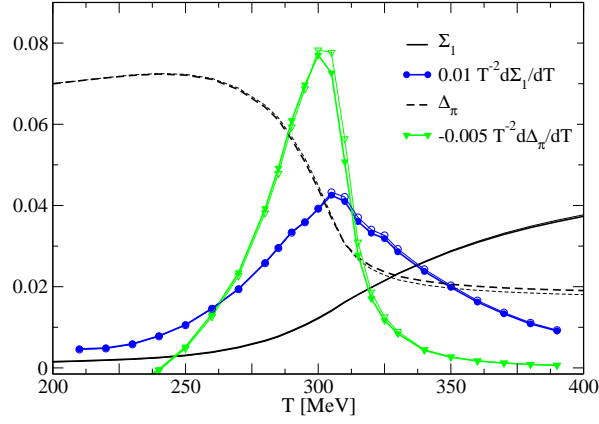


FIG. 7: Temperature dependence of the dressed Polyakov-loop Σ_1 and the conventional quark condensate $\Delta_\pi \equiv \langle \bar{\psi}\psi \rangle_{\varphi=\pi}$ together with their derivatives for $m = 10$ MeV in the infinite volume/continuum limit. The thick lines, already shown in the right diagram of Fig. 3, correspond to the decoupling type of interaction whereas the thin lines are the scaling type of interaction Eqs. (C1), (C2) and (C3).

vertex in the quenched theory is also given by a power law [42] and can be represented by the ansatz

$$\Gamma_\nu^{scaling}(q, k, p) = \Gamma_\nu(q, k, p) \left(\frac{q^2}{q^2 + \Lambda_{IR}^2} \right)^{-1/2-\kappa} \quad (C3)$$

where q is the gluon momentum and $\Gamma_\nu(q, k, p)$ is given by Eq. (11).

Our numerical solutions for the quark condensate and the dressed Polyakov loop are given in Fig. 7. The results with decoupling type of interaction already given in Fig. 3 in the main body of this work are shown together with the results obtained from the scaling type of inter-

action. The differences are tiny. Below the transitions the effects are not visible. Here the dynamically generated quark mass in the quark-DSE shields the interaction in the deep infrared; the results are independent of the behavior of the interaction below Λ_{IR} . We also find the same transition temperatures for both types of solutions. In the high temperature phase where chiral symmetry is partly restored we observe small effects in the ordinary condensate and almost no effect in the dual chiral condensate. The main aspects of the two transitions are not concerned. Whether there is some impact on the properties of quarks within the quark-gluon plasma remains to be investigated.

-
- [1] A. M. Polyakov, Phys. Lett. B **72** (1978) 477; L. Susskind, Phys. Rev. D **20**, 2610 (1979).
- [2] F. Karsch and E. Laermann, arXiv:0305025 [hep-lat].
- [3] Y. Aoki, Z. Fodor, S. D. Katz and K. K. Szabo, Phys. Lett. B **643** (2006) 46 [arXiv:hep-lat/0609068].
- [4] A. Bazavov *et al.*, Phys. Rev. D **80** (2009) 014504 [arXiv:0903.4379 [hep-lat]].
- [5] Y. Aoki, S. Borsanyi, S. Durr, Z. Fodor, S. D. Katz, S. Krieg and K. K. Szabo, JHEP **0906**, 088 (2009) [arXiv:0903.4155 [hep-lat]].
- [6] J. Greensite, Prog. Part. Nucl. Phys. **51** (2003) 1 [arXiv:hep-lat/0301023].
- [7] J. Gattnar, C. Gattringer, K. Langfeld, H. Reinhardt, A. Schafer, S. Solbrig and T. Tok, Nucl. Phys. B **716**, 105 (2005) [arXiv:hep-lat/0412032].
- [8] C. Gattringer, Phys. Rev. Lett. **97** (2006) 032003, [arXiv:hep-lat/0605018].
- [9] F. Bruckmann, C. Gattringer and C. Hagen, Phys. Lett. B **647** (2007) 56, [arXiv:hep-lat/0612020].
- [10] F. Synatschke, A. Wipf and C. Wozar, Phys. Rev. D **75** (2007) 114003, [arXiv:hep-lat/0703018].
- [11] F. Synatschke, A. Wipf and K. Langfeld, Phys. Rev. D **77** (2008) 114018, [arXiv:0803.0271 [hep-lat]].
- [12] E. Bilgici, F. Bruckmann, C. Gattringer and C. Hagen, Phys. Rev. D **77** (2008) 094007, [arXiv:0801.4051].
- [13] F. Bruckmann, C. Hagen, E. Bilgici and C. Gattringer, PoS **LATTICE2008** (2008) 262, [arXiv:0810.0899].
- [14] J. Danzer, C. Gattringer and A. Maas, JHEP **0901** (2009) 024, [arXiv:0810.3973 [hep-lat]].
- [15] E. Bilgici, F. Bruckmann, J. Danzer, C. Gattringer, C. Hagen, E. M. Ilgenfritz and A. Maas, arXiv:0906.3957 [hep-lat].
- [16] C. S. Fischer, Phys. Rev. Lett. **103**, 052003 (2009), arXiv:0904.2700 [hep-ph].
- [17] A. Cucchieri, A. Maas and T. Mendes, Phys. Rev. D **75**, 076003 (2007), [arXiv:hep-lat/0702022].
- [18] J. Braun, H. Gies and J. M. Pawłowski, arXiv:0708.2413 [hep-th]; F. Marhauser and J. M. Pawłowski, arXiv:0812.1144 [hep-ph].
- [19] J. Braun, L. Haas, F. Marhauser and J. M. Pawłowski, arXiv:0908.0008 [hep-ph].
- [20] A. Roberge and N. Weiss, Nucl. Phys. B **275** (1986) 734.
- [21] R. Williams, C. S. Fischer and M. R. Pennington, Phys. Lett. B **645** (2007) 167 [arXiv:hep-ph/0612061]; arXiv:0704.2296 [hep-ph].
- [22] C. D. Roberts and S. M. Schmidt, Prog. Part. Nucl. Phys.

- 45, S1 (2000), [arXiv:nucl-th/0005064].
- [23] C. S. Fischer, A. Maas and J. M. Pawłowski, *Annals Phys.* **324**, 2408 (2009) [arXiv:0810.1987 [hep-ph]].
- [24] A. Maas, J. Wambach and R. Alkofer, *Eur. Phys. J. C* **42** (2005) 93, [arXiv:hep-ph/0504019];
- [25] A. Sternbeck, E. M. Ilgenfritz, M. Müller-Preussker, A. Schiller and I. L. Bogolubsky, *PoS LAT2006* (2006) 076 [arXiv:hep-lat/0610053].
- [26] J. S. Ball and T. W. Chiu, *Phys. Rev. D* **22** (1980) 2542.
- [27] C. S. Fischer and R. Williams, *Phys. Rev. D* **78** (2008) 074006, [arXiv:0808.3372 [hep-ph]].
- [28] A. Bender, D. Blaschke, Y. Kalinovsky and C. D. Roberts, *Phys. Rev. Lett.* **77** (1996) 3724, [arXiv:nucl-th/9606006].
- [29] P. Maris, C. D. Roberts, S. M. Schmidt and P. C. Tandy, *Phys. Rev. C* **63**, 025202 (2001) [arXiv:nucl-th/0001064].
- [30] D. Horvatic, D. Klabucar and A. E. Radzhabov, *Phys. Rev. D* **76** (2007) 096009 [arXiv:0708.1260 [hep-ph]].
- [31] C. S. Fischer, R. Alkofer and H. Reinhardt, *Phys. Rev. D* **65** (2002) 094008, [arXiv:hep-ph/0202195]; C. S. Fischer and M. R. Pennington, *Phys. Rev. D* **73** (2006) 034029, [arXiv:hep-ph/0512233]; C. S. Fischer, A. Maas, J. M. Pawłowski and L. von Smekal, *Annals Phys.* **322** (2007) 2916. [arXiv:hep-ph/0701050].
- [32] F. Karsch, arXiv:hep-lat/9903031.
- [33] J. Fingberg, U. M. Heller and F. Karsch, *Nucl. Phys. B* **392** (1993) 493; [arXiv:hep-lat/9208012]. O. Kaczmarek, F. Karsch, P. Petreczky and F. Zantow, *Phys. Lett. B* **543** (2002) 41; [arXiv:hep-lat/0207002]. B. Lucini, M. Teper and U. Wenger, *JHEP* **0502** (2005) 033;
- [34] R. Alkofer, C. S. Fischer and F. J. Llanes-Estrada, *Phys. Lett. B* **611**, 279 (2005) [arXiv:hep-th/0412330].
- [35] C. S. Fischer and J. M. Pawłowski, *Phys. Rev. D* **75**, 025012 (2007) [arXiv:hep-th/0609009]; *Phys. Rev. D* **80**, 025023 (2009) [arXiv:0903.2193 [hep-th]].
- [36] R. Alkofer, M. Q. Huber and K. Schwenzer, arXiv:0801.2762 [hep-th];
- [37] Ph. Boucaud, J. P. Leroy, A. L. Yaouanc, J. Micheli, O. Pene and J. Rodriguez-Quintero, *JHEP* **0806**, 012 (2008) [arXiv:0801.2721 [hep-ph]].
- [38] A. C. Aguilar, D. Binosi and J. Papavassiliou, *Phys. Rev. D* **78**, 025010 (2008) [arXiv:0802.1870 [hep-ph]].
- [39] T. Kugo and I. Ojima, *Prog. Theor. Phys. Suppl.* **66**, 1 (1979) [Erratum *Prog. Theor. Phys.* **71**, 1121 (1984)]; T. Kugo, arXiv:hep-th/9511033.
- [40] C. Lerche and L. von Smekal, *Phys. Rev. D* **65**, 125006 (2002) [arXiv:hep-ph/0202194]; J. M. Pawłowski, D. F. Litim, S. Nedelko and L. von Smekal, *Phys. Rev. Lett.* **93**, 152002 (2004) [arXiv:hep-th/0312324].
- [41] D. Zwanziger, *Phys. Rev. D* **65**, 094039 (2002) [arXiv:hep-th/0109224];
- [42] R. Alkofer, C. S. Fischer, F. J. Llanes-Estrada and K. Schwenzer, *Annals Phys.* **324**, 106 (2009) [arXiv:0804.3042 [hep-ph]];